Coordination Chemistry Reviews, 64 (1985) 207—224
Elsevier Science Publishers B.V., Amsterdam — Printed in The Netherlands

PHOTOELECTROCHEMISTRY OF METALLOCHLOROPHYLLS

T. WATANABE,[1] K. MACHIDA,[1] H. SUZUKI,[1] M. KOBAYASHI,[1] and K. HONDA[1,2]

[1]Department of Synthetic Chemistry, Faculty of Engineering, University of Tokyo, Hongo, Bunkyo-ku, Tokyo 113 (Japan)

[2]Division of Molecular Engineering, Faculty of Engineering, Kyoto University, Yoshida, Sakyo-ku, Kyoto 606 (Japan)

ABSTRACT

Photoinduced electron transfer from eleven metallochlorophyll *a* (M-Chl *a*) monolayers to a SnO_2 substrate was investigated photoelectrochemically. Six M-Chl *a*s [M = Pd(II), Cu(II), Hg(II), H_2(II), Mg(II), and Zn(II)] gave measurable photoeffects. For the latter three pigments, two-dimensional dilution of the monolayer led to an enhancement of the photocurrent quantum yield. The highest quantum yield was attained with Mg-Chl *a* at sufficient dilution. Five M-Chl *a*s [M = Ni(II), Co(II), Ag(II), Mn(III), and Fe(III)] showed no photoresponse, due probably to a rapid intramolecular deactivation of the excited state. Some kinetic aspects of the interfacial photoprocess were clarified by experiments with mixed monolayers composed of a photoactive M-Chl *a* and photo-inactive Ni-Chl *a* (quencher).

INTRODUCTION

In the primary process of green plant photosynthesis, solar energy is absorbed by the so-called antenna pigment system and is then channelled to the as yet unidentified reaction center, where charge separation takes place with a quantum yield reaching unity. The main component of both the antenna system and the reaction center is chlorophyll (Chl) *a*, which is a magnesium complex of substituted chlorin macrocycle. To date, the role of the central Mg atom in driving photosynthesis has not been thoroughly clarified. In view of this, it is of much interest to systematically compare the photoredox properties, as well as other physicochemical properties, of a series of metallochlorophylls* (M-Chls).

Several workers have studied M-Chls so far. But these studies were mainly in connection with metallation-demetallation kinetics (refs. 1 and 2), identification of the formation pathway of metal complexes found in fossil fuels (ref. 3), or pigment alteration during vegetable processing (ref. 4). Thus, as far as we are aware, the photophysical and redox characteristics of M-Chls have not been

* We prefer the term "metallochlorophylls" to a more strict term "metallopheophytins" (pheophytin = metal-free Chl) because the naturally occurring Chl *a* is often called Mg-Chl *a*. In this context the pheophytin *a* itself is referred to as H_2-Chl *a*.

0010-8545/85/$06.30

reported.

In photosynthetic apparatus the Chl molecules are supposed to exist in the form of organized assemblies. Such molecular assemblies are constructed through interactions of neighboring Chl molecules via the peripheral substituents on the chlorin ring (in particular, the two carbonyl groups on the cyclopentanone ring. cf. Fig. 1) as well as the central Mg atom (ref. 5). In order to extract useful information on the *in vivo* function of Mg from *in vitro* experiments with M-Chls, it is hence essential to prepare M-Chl samples by keeping intact the whole molecular structure except for the central metal. However, the peripheral substituents of M-Chls are fairly labile; they tend to undergo various alterations depending on the chemical environment and temperature (ref. 6), and yet most of such altered products are hardly distinguishable from the genuine M-Chl by simple visible absorption spectroscopy. For instance, our attempt (ref. 7) to synthesize Pd-Chl *a* by a reaction of H_2-Chl *a* with $PdCl_2$ in deoxygenated glacial acetic acid at 60 °C for 36 h gave (as verified by HPLC analysis) a mixture of at least ten different compounds. The mixture did not contain the authentic Pd-Chl *a* any more, but exhibited an absorption spectrum practically identical with that of Pd-Chl *a* prepared under much milder conditions. Previous authors occasionally prepared M-Chls by solution phase reaction under boiling (refs. 3 and 8); hence the purity (in the sense of molecular integrity) of their samples is somewhat questionable.

In the present work we compared the efficiencies of photoinduced electron transfer from eleven M-Chl *a*s to the conduction band of SnO_2 in an electrochemical

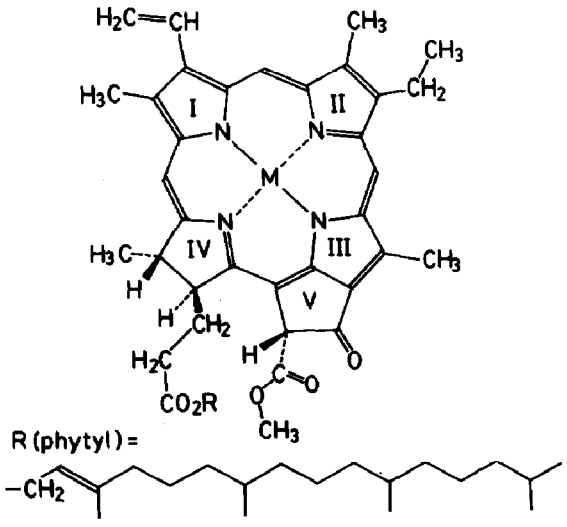

Fig. 1 Structural formula for a M-Chl *a*. For a trivalent M, an anion (chloride or acetate) is attached to fulfill the electrical neutrality.

system. The molecular integrity of M-Chl *a* samples was assured rigorously. By depositing M-Chl *a* on a SnO_2 electrode by means of the Langmuir-Blodgett technique to obtain a monomolecular layer with controlled orientation and intermolecular separation, anodic photocurrents were measured by visible excitation of the deposited monolayer. This experiment could therefore place the naturally occurring Mg-Chl *a* among a series of M-Chl *a*s with respect to the electron-releasing capability at the excited state. It is also expected that a systematic comparison between the photoelectrochemical activity and the physicochemical properties of M-Chl *a*s could provide a clue for devising an artificial system for solar energy conversion.

EXPERIMENTAL

Sample Preparation

M-Chl *a*s were synthesized by metallation of pheophytin *a* (H_2-Chl *a*) with metal salts (chloride or acetate) in glacial acetic acid or ethanol at room temperature. The products were purified by preparative-scale high-performance liquid chromatography (HPLC), and their molecular integrity was confirmed by elemental analysis. The details for the synthetic procedure will be described elsewhere (ref. 7). Of the fifteen M-Chl *a*s thus synthesized, eleven [M = H_2(II), Mg(II), Mn(III), Fe(III), Co(II), Ni(II), Cu(II), Zn(II), Pd(II), Ag(II), and Hg(II)] were employed in the present photoelectrochemical measurements.

Physicochemical Characterization of M-Chl *a*s

The M-Chl *a*s thus prepared have been characterized for visible absorption and fluorescence (ref. 7), phosphorescence (ref. 8), electrochemical and spectroelectrochemical properties (ref. 9), and intermolecular aggregation behaviors

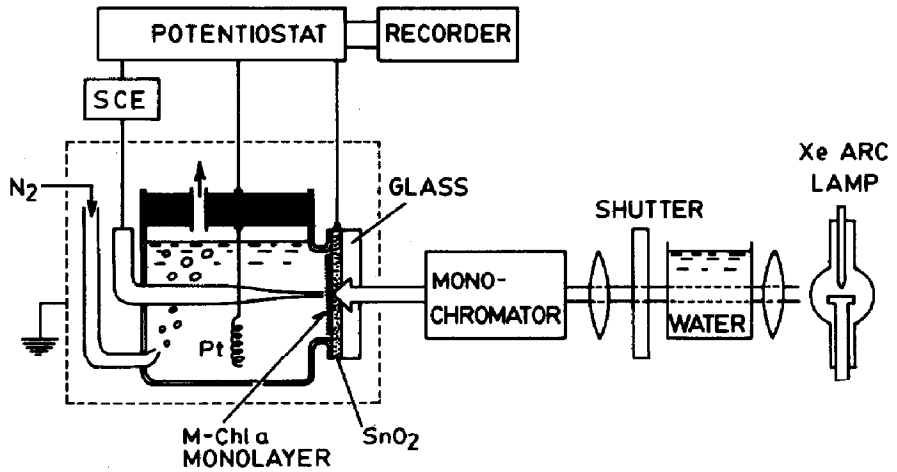

Fig. 2 Schematic illustration of the photoelectrochemical measurement setup.

(ref. 10). The results of these characterizations, though they still remain to be published, will be mentioned in relevant parts below.

Deposition of Monomolecular Layers

A monomolecular layer of M-Chl *a* was deposited on a 3 x 3 cm SnO_2 electrode by means of the Langmuir-Blodgett method (refs. 11 and 12). The electrode was made of a 1-mm thick glass plate carrying a SnO_2 film, the thickness of which is 2000 Å unless otherwise noted. It is supposed that within a M-Chl *a* monolayer the hydrophilic moieties (a keto carbonyl and two ester carbonyls, see Fig. 1) in the molecule are attached to the hydrophilic SnO_2 surface and that the hydrophobic phytyl chain and chlorin ring direct themselves outward from the surface. The surface pressure during deposition was regulated to 20 dynes cm^{-1} in all cases. In experiments with controlled surface concentration of M-Chl *a*, dipalmitoyl L-α-phosphatidylcholine (or dipalmitoyl lecithin, DPL) was used as a two-dimensional diluent.

Photoelectrochemical Measurements

Figure 2 schematically shows the experimental setup for photocurrent measurements. The working electrode is a M-Chl *a*-deposited SnO_2 plate attached as a window of the electrochemical cell. The electrode potential is set at a value giving a maximum anodic photocurrent, and is in a range from +0.05 to +0.1 V vs. SCE (saturated calomel electrode, used as reference) for most M-Chl *a*s. Light from a 500-W xenon arc lamp passes successively through a water filter for IR removal and a grating monochromator and excites the M-Chl *a* monolayer in contact with an electrolyte solution. The latter contains 0.1 M Na_2SO_4 as a supporting electrolyte and 0.05 M hydroquinone as a reducing agent (to prevent oxidative degradation of M-Chl *a*), and is flushed with deoxygenated nitrogen gas to remove dissolved oxygen. The quantum yield of anodic photocurrent is calculated on the basis of the number of photons absorbed by the M-Chl *a* monolayer, which in turn is obtained from the measured incident photon flux and the absorbance of the monolayer.

RESULTS AND DISCUSSION

Monomolecular Layer Formation

All the eleven M-Chl *a*s formed a well-behaved monomolecular layer on the SnO_2 substrate, with an *F*(surface pressure) - *A*(area per molecule) curve similar to that of Mg-Chl *a* reported previously (ref. 12). Qualitatively this assures the presence of the phytyl chain in the molecule, because otherwise the state of packing of the monolayer would undergo a drastic change. As an example, the visible absorption spectrum of a Cu-Chl *a* monolayer is given in Fig. 3. (To avoid absorption by SnO_2 in the near-UV, a Pyrex glass is used here as the substrate.) The red absorption peak shows a slight bathochromic shift from 551 nm in acetone

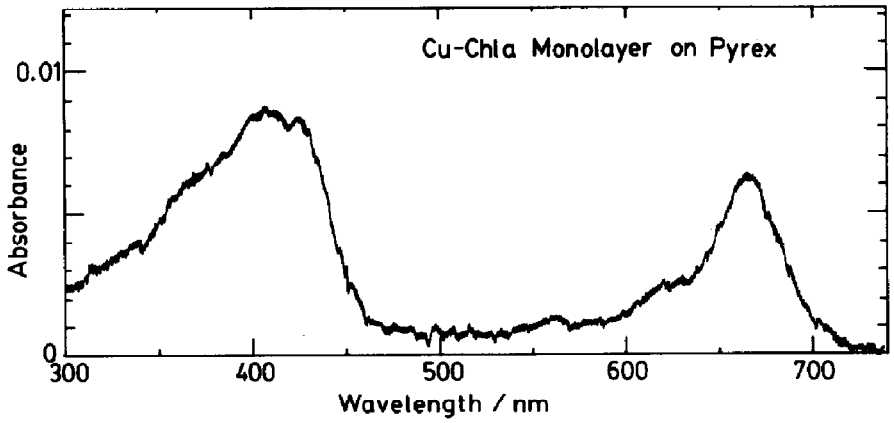

Fig. 3 Absorption spectrum of a Cu-Chl *a* monomolecular layer.

to 665 nm on the SnO_2 surface. The absorbance at the red peak (0.006) corresponds to a surface concentration of 5.6×10^{13} molecules cm^{-2} under the assumption that the molar absorption coefficient of Cu-Chl *a* be common in acetone (64200 $M^{-1}cm^{-1}$) and at the adsorbed state.

Anodic Photocurrent Quantum Yields for M-Chl *a* Compact Monolayers

The M-Chl *a* monolayers deposited at a surface pressure of 20 dynes cm^{-1} are in a highly packed state, with an average intermolecular separation of 7 - 10 Å. Of the eleven M-Chl *a*s examined, only six (M = Pd, Cu, Hg, H_2, Mg, and Zn) gave anodic photocurrents by visible excitation under these conditions. In what follows, the anodic photocurrent observed by M-Chl *a* excitation is referred to as the sensitized photocurrent, i_s. Further, the photocurrent quantum yield Φ_s is defined by the ratio of the number of electrons flowing in the external circuit to the number of photons absorbed by M-Chl *a* monolayer at the red absorption peak.

Figure 4 shows the action spectra of i_s for the six (sensitizing) M-Chl *a*s. The shape of each action spectrum generally coincided with that of the absorption spectrum of the monolayer. The peak positions are slightly red-shifted from the absorption peaks in acetone solutions (631 nm for Pd-Chl *a*, 651 nm for Cu-Chl *a*, 678 nm for Hg-Chl *a*, 668 nm for H_2-Chl *a*, 663 nm for Mg-Chl *a*, and 655 nm for Zn-Chl *a*. ref. 7). In Fig. 4 the level of i_s has been corrected for (a) the spectral intensity distribution of the light source and (b) the absorbance at the red maximum of each M-Chl *a* monolayer. Hence the height of the peaks gives the relative values of the quantum yield Φ_s. The classification of the six M-Chl *a*s into two groups in Fig. 4 is based on the difference in photophysical and intermolecular aggregation characteristics, which in turn are reflected by the difference in the behavior of Φ_s by two-dimensional dilution of the monolayer, as will be explained later.

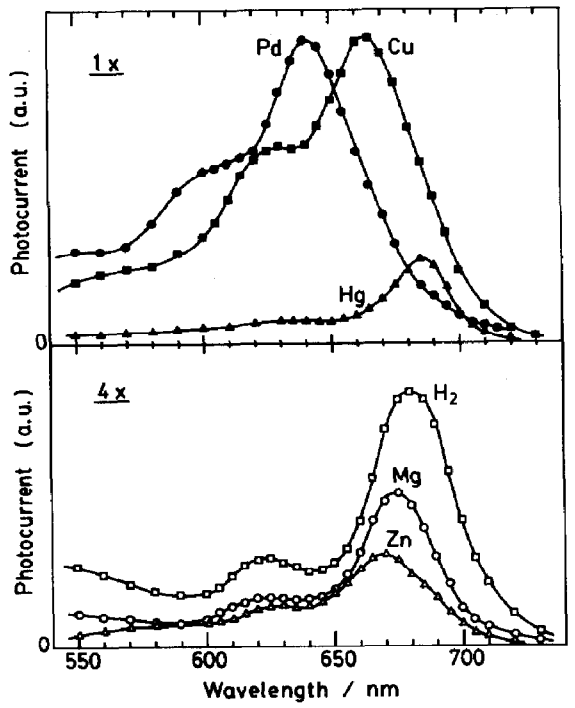

Fig. 4 Action spectra for the anodic photocurrent observed at M-Chl a compact monolayer / SnO_2 interfaces. The peak height represents the relative quantum yield. The lower three curves are fourfold magnified.

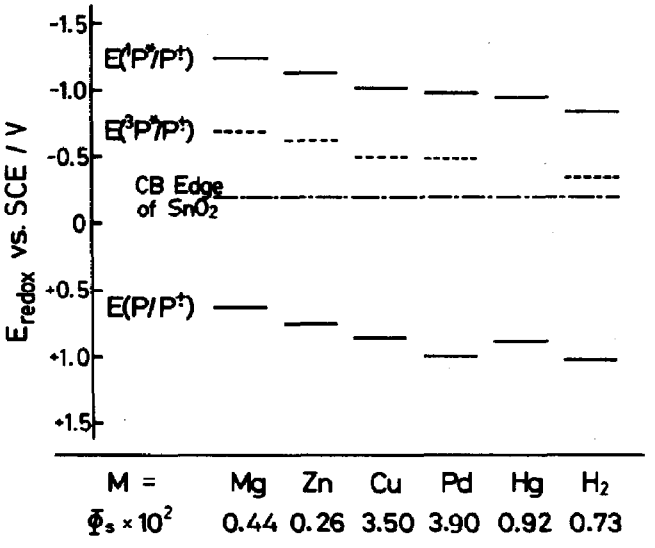

Fig. 5 Diagram showing the photocurrent quantum yield Φs and the energetic conditions at M-Chl a / SnO_2 interfaces. $E(P/P^+)$, $E(^1P^*/P^+)$, and $E(^3P^*/P^+)$ are the oxidation (electron-releasing) redox potentials at the ground state, singlet excited state, and triplet excited state, respectively.

In Fig. 5, the absolute values of Φ_s for compact monolayers of the six M-Chl*a*s are presented in comparison with the M-Chl *a* / SnO_2 interfacial energetics. The level of the conduction band (CB) edge of the SnO_2 electrode (-0.25 V vs. SCE) was determined by measurements of interfacial capacitance in an electrolyte solution of pH 7.0 (ref. 12). The $E(P/P^{+})$ levels are the reversible oxidation potentials of ground-state M-Chl *a*s as obtained by cyclic voltammetry in organic solvents (ref. 9). Shifting the $E(P/P^{+})$ levels vertically by the singlet excitation energy (midpoint energy between the absorption and fluorescence maxima, ref. 7) or by the triplet excitation energy (phosphorescence peak energy, ref. 8) gives $E(^1P^*/P^{+})$ or $E(^3P^*/P^{+})$ levels, respectively. For non-fluorescent Cu-Chl *a* and Hg-Chl *a*, the red absorption peak energy was used as the singlet excitation energy. It is seen that the energetic requirements for electron transfer from either the singlet or triplet excited state to the conduction band of SnO_2 are fulfilled for all the six M-Chl *a*s. A simple energetic consideration would predict a higher value of Φ_s for a M-Chl *a* having more negative redox levels. However, the order of Φ_s does not parallel that of the energetic position of M-Chl *a* excited levels.

In this context we note that a fairly good parallelism exists between the Φ_s and the $E(P/P^{+})$ level for a total of eight M-TPPs (TPP = tetraphenylporphyrin) at an Al/TPP interface, as reported by Kampas et al. (ref. 13). An essential difference between M-Chl *a*s and the artificial M-TPPs is that the latter compounds lack peripheral substituents which could lead to strong coordination interactions between neighboring molecules. Therefore, the cause for the absence of a direct correlation between Φ_s and energy levels should be sought in intermolecular interactions within the M-Chl *a* monolayers.

As mentioned above, each M-Chl *a* has an adjacent molecule at a distance of 7 - 10 Å in a compact monolayer. If the M-Chl *a* molecule is fluorescent, we could expect the occurrence of a very efficient singlet-singlet excitation energy migration within the monolayer according to the Förster resonance mechanism. Excitation energy migration *per se*, however, does not influence the net efficiency of electron injection into the conduction band of the substrate. The situation could change drastically if the M-Chl *a* molecules form dimers or aggregates, since aggregated states generally (1) show higher rates of intramolecular deactivation of the excitation energy due to increased number of vibrational modes and (2) absorb at longer wavelengths than monomers. Thus aggregates tend to act as energy traps in the monolayer. These considerations point to the importance of two parameters, namely the fluorescence properties and aggregation behaviors of M-Chl *a*s, in determining the value of Φ_s at the M-Chl*a*/ SnO_2 interface.

Physicochemical characterization of M-Chl *a*s (refs. 7 and 10) gave the following results. Mg-, Zn-, and H_2-Chl *a* are highly fluorescent, with a fluorescence quantum yield Φ_f (measured in deoxygenated benzene) ranging from 0.23 to 0.30.

Pd-Chl *a* is weakly fluorescent ($\Phi_f = 0.0025$), and other M-Chl *a*s are essentially non-fluorescent. Aggregation behaviors of M-Chl *a*s were evaluated following a procedure described by Uehara et al. (ref. 14). Thus, M-Chl *a* was solubilized in an aqueous solution containing 0.1 wt.% poly(vinyl alcohol) and the evolution of visible absorption spectrum was measured. Mg- and Zn-Chl *a* seemed to form large aggregates, characterized by the appearance of a new absorption peak at respectively 735 and 726 nm, which are red-shifted by as much as 60 nm from the monomer absorption peaks. Judging from a difference in the velocity of the spectral change, the aggregation tendency of Zn-Chl *a* is much higher than that of Mg-Chl *a*. H_2- and Ag-Chl *a* exhibited a 10-nm bathochromic shift which was completed in *ca.* 90 and 400 min, respectively. This is suggestive of the formation of π-dimers. For Cu-, Co-, and Ni-Chl *a*, a new peak or shoulder appeared at wavelengths in a range of 680-700 nm, possibly reflecting the formation of dimers or trimers. In these cases the spectral change was extremely slow, and was barely detectable in 1-2 h. These three M-Chl *a*s can thus be regarded as non-aggregating during the photocurrent measurements. Finally, Pd-, Hg-, and Mn-Chl *a* showed no trend toward dimerization or aggregation in a time range of 7-8 h.

These results reveal a significant influence of the central metal on the photophysical properties and intermolecular coordination interactions of M-Chl *a*s. On this basis, we could classify the six sensitizing M-Chl *a*s (Figs. 4 and 5) into two groups:

Group I : Mg-, Zn-, and H_2-Chl *a*, which are strongly fluorescent and, at the same time, possess a high tendency toward aggregation.

Group II: Cu- and Hg-Chl *a*, which are neither fluorescent nor aggregating, and Pd-Chl *a*, which is weakly fluorescent but non-aggregating.

According to the foregoing arguments, the Φ_s value for Group I M-Chl *a*s should be lowered due to the occurrence of energy transfer, accompanied by energy trapping at dimer or aggregate sites present in a compact monolayer. The relatively low values for Mg-, Zn-, and H_2-Chl *a* observed experimentally (Fig. 5) could be rationalized in this way.

Concerning the so-called antenna or light-harvesting pigment system in plant photosynthesis, it is supposed that a highly efficient Förster-type energy transfer takes place to channel the absorbed light energy to reaction centers. Nevertheless, the quantum yield for the initial charge separation *in vivo* is nearly 100%. This strongly indicates the presence of some particular arrangement of antenna Mg-Chl *a* molecules such that the intermolecular aggregation is effectively hindered.

Dependence of the Photocurrent Quantum Yield on M-Chl *a* Surface Concentration

By using DPL as a two-dimensional diluent of the monolayer, the value of Φ_s

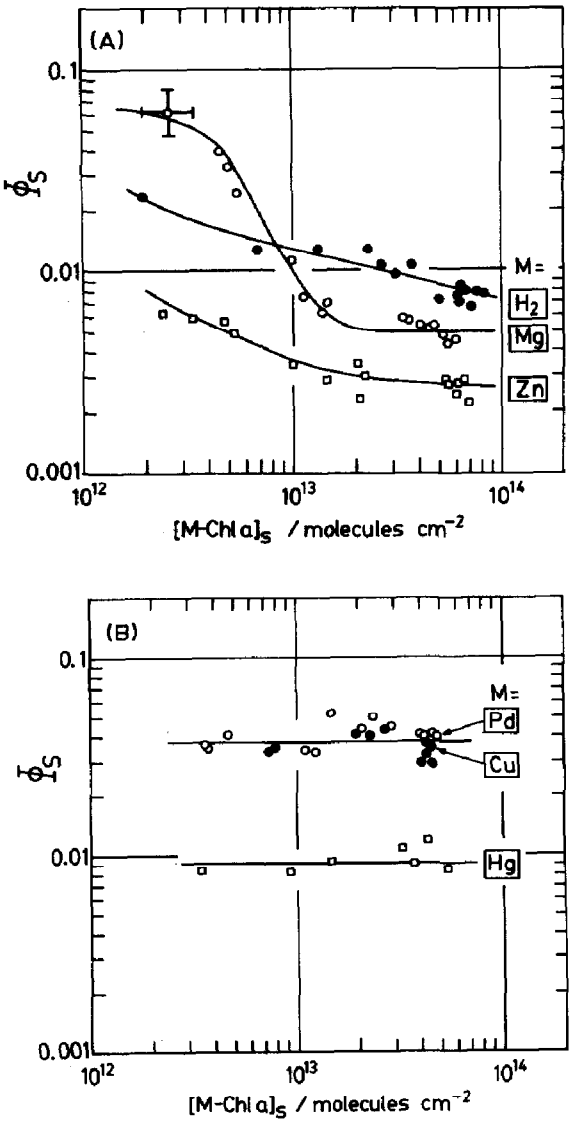

Fig. 6 Dependence of the photocurrent quantum yield Φ_s on the surface concentration of M-Chl *a*, $[M\text{-}Chl\,a]_s$

has been measured as a function of M-Chl *a* surface concentration. The results are displayed in Fig. 6. The right-hand end [$(5\text{-}8) \times 10^{13}$ molecules cm^{-2}] corresponds to the compact monolayer. Owing to a difficulty in recording the monolayer absorbance, the measurements were limited to surface concentrations higher than 2×10^{12} molecules cm^{-2}. Figure 6A clearly shows that, for Group I M-Chl *a*s (see above), dilution of the monolayer leads to an enhancement of the photocurrent quantum yield. This behavior is understood by invoking a decrease in both aggregation and energy transfer with increasing intermolecular separation. At

surface concentrations above 3×10^{13} molecules cm^{-2}, dimers or small aggregates are most probably the dominant species for these three M-Chl *a*s. The tenfold increase in the Φ_s value of Mg-Chl *a* in going from 2×10^{13} to 3×10^{12} molecules cm^{-2} may hence indicate the occurrence of dimer $\rightarrow$ monomer conversion in this concentration range. The Φ_s values for H_2- and Zn-Chl *a* tend to increase only slowly by two-dimensional dilution. This may reflect the stronger intermolecular association capabilities of these pigments (see above) as compared with Mg-Chl *a*. That this slow increase in Φ_s comes indeed from disaggregation, is verified by a gradual shift of the photocurrent peak wavelength of H_2-Chl *a* as a function of surface concentration (in molecules cm^{-2}): 683 nm at 7.9×10^{13}, 680 nm at 6.8×10^{13}, 678 nm at 3.2×10^{13}, and 675 nm at 1.3×10^{13}.

For Group II M-Chl as (Fig. 6B), the Φ_s value does not depend noticeably on the surface concentration, as expected from the foregoing arguments. The non-fluorescent Cu- and Hg-Chl *a* are supposed to inject an electron to the CB of SnO_2 from the triplet excited state. For Pd-Chl *a*, the fluorescence emission rate constant k_f is estimated to be about 2×10^{10} s^{-1} from the observed fluorescence quantum yield (0.0025) and the calculated natural fluorescence lifetime of Chl *a* (20 ns). Therefore, depending on the rate constant for electron transfer, Pd-Chl *a* could inject an electron to SnO_2 from either singlet or triplet excited state. This point will be discussed later.

Deactivation Pathways at the M-Chl *a*/SnO_2 Interface

The values of Φ_s observed at M-Chl *a* / SnO_2 interfaces are fairly low, the maximum being 5-8% for a sufficiently dilute Mg-Chl *a* monolayer (Fig. 6A). This points to the presence of an efficient route to deactivation. [We must admit that the high Φ_s values reported in a preliminary account of this work (ref. 15) resulted from some errors in calculation.] Since the energetic conditions are quite favorable for electron transfer at the interface (Fig. 5), we suppose that whereas the initial electron injection into SnO_2 is a very efficient process, the injected electron recombines rapidly back with the M-Chl *a* cation radical before the latter is reduced by hydroquinone added in the electrolyte solution. The rate of such a recombination will depend strongly on the nature of the space charge layer (SCL) of the SnO_2 surface, where the electron finds itself just after injection.

In most experiments we used a glass plate carrying a 2000-Å thick SnO_2 film as the working electrode. The film thickness may not be uniform over the entire 3 x 3 cm area. Although the thickness of the SCL is typically 10-20 Å for the SnO_2 electrode employed (ref. 12), it may happen that the thickness of a part of the film is not enough to sustain the whole SCL if the average SnO_2 film thickness is too small. Such a situation would lead to lowering of Φ_s. To check for this possibility, we measured the Φ_s value for a compact monolayer of Cu-Chl *a* depos-

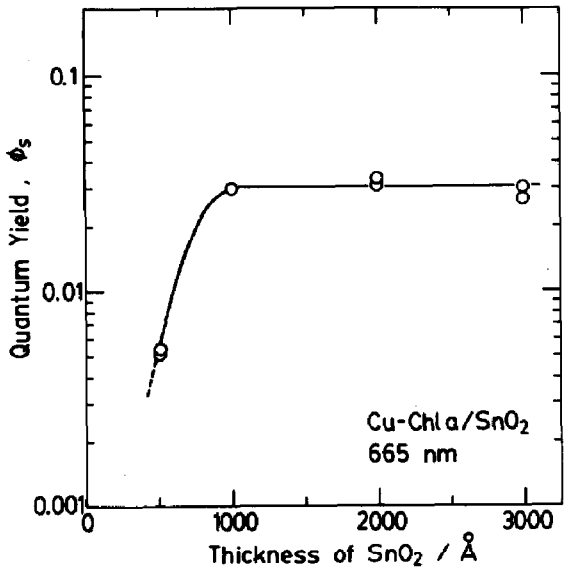

Fig. 7 Dependence of the photocurrent quantum yield Φs on the SnO_2 film thickness for a Cu-Chl *a* compact monolayer.

ited on 500, 1000, 2000, and 3000-Å thick SnO_2 electrodes. The result, depicted in Fig. 7, indicates that the SnO_2 thickness is not rate-determining at thicknesses larger than 1000 Å. (The significantly low quantum yield observed at a 500-Å thick electrode may be, as stated above, due to a non-uniformity of the SnO_2 film.) Another, probably more important factor affecting the net quantum yield is the potential gradient within the SCL, which in turn is controlled by the doping level of the semiconductor. A recent work (ref. 16) indeed demonstrates a drastic effect of the electrode donor density on the Φ_s value for sensitization of SnO_2 electrodes with synthetic dyes, Rhodamine B and Rose Bengal. Therefore, we could expect that the Φ_s value for the M-Chl *a* / SnO_2 interfaces also would be considerably enhanced by controlling the doping level of the SnO_2 electrode.

Non-Sensitizing M-Chl *as*

Of the eleven M-Chl *as* examined, Ni-, Co-, Ag-, Mn-, and Fe-Chl *a* gave no sensitized photocurrent on the SnO_2 electrode. This was true for both compact and diluted monolayers. As far as the optical absorption property is concerned, no anomaly is noted for these five pigments. For example, both the "sensitizing" Cu-Chl *a* and "non-sensitizing" Ag-Chl *a* possess quite similar absorption spectra characteristic of the π-π^* transition within the chlorin macrocycle, as shown in Fig. 8. The five non-sensitizing M-Chl *as* are totally non-fluorescent, but this property cannot be related to the inability of photoinduced electron transfer

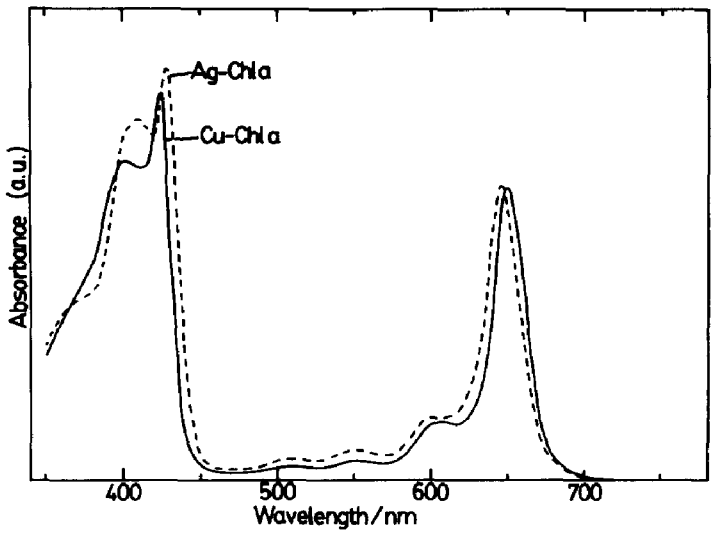

Fig. 8 Visible absorption spectra of Cu- and Ag-Chl *a* in acetone.

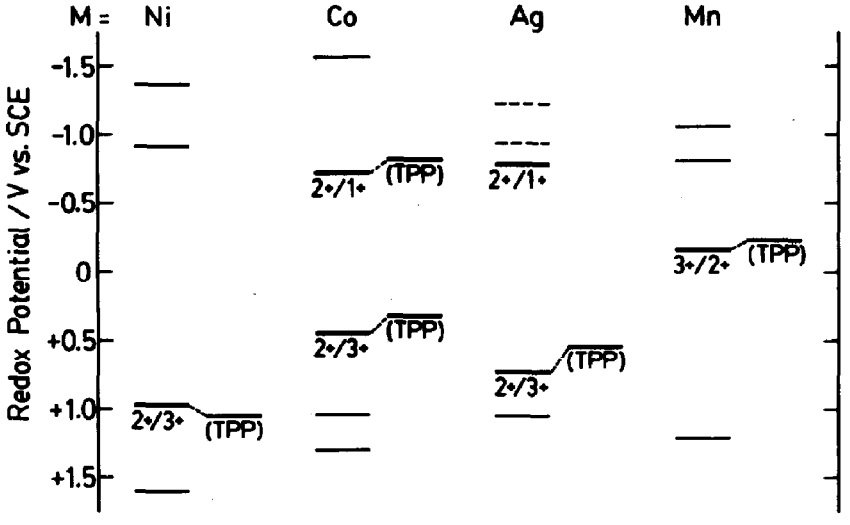

Fig. 9 Redox potentials of four non-sensitizing M-Chl as determined by cyclic voltammetry in butyronitrile (ref. 9). The lettered levels represent redox reactions of the central metal ions. The levels denoted TPP are the corresponding redox levels for M-tetraphenylporphyrins (ref. 18). Ag(II)-Chl *a* undergoes demetallation on Ag(II) → Ag(I) reduction (ref. 9); hence the two dashed reduction levels are the first and second reduction potentials for the chlorin ring of H_2-Chl *a*.

since non-fluorescent Cu- and Hg-Chl *a* are fairly good sensitizers.

Spectroelectrochemical characterization of M-Chl as (ref. 9) has brought to light an interesting feature common to all the non-sensitizing M-Chl as. The

method consists of examining, based on the criteria established empirically for a series of metalloporphyrins (refs. 17 and 18), the pattern of spectral change upon oxidation or reduction of M-Chl *a*s by means of the thin-layer electrolysis technique (refs. 19 and 20). The results gave clear evidence that the five non-sensitizing M-Chl *a*s exhibit redox reactions of the central metal ion in a fairly mild potential range, as illustrated in Fig. 9. (Fe-Chl *a*, not shown here, also possesses a redox wave corresponding to the Fe(II)/Fe(III) interconversion.) In sharp contrast, the six sensitizing M-Chl *a*s (Fig. 5) undergo redox reactions exclusively on the chlorin macrocycle. The ease, in the five non-sensitizing M-Chl *a*s, of the metal redox reaction would lead to an efficient electron exchange between the central metal ion and the π-π^* excited chlorin ring. We therefore suppose that the non-sensitizing property of Ni-, Co-, Ag-, Mn-, and Fe-Chl *a* results from a very rapid quenching of the π-π^* excited state via an intramolecular charge-transfer process. Another possibility may be the quenching of the π-π^* excited state through intramolecular energy transfer to low-lying d-d levels of the central metal ion. The occurrence of an extremely fast nonradiative decay in a Ni-porphyrin has indeed been demonstrated by Kobayashi et al. (ref. 21), who observed that the singlet excited state of Ni-protoporphyrin IX dimethyl ester is quenched intramolecularly with a time constant of 10 ± 2 ps.

It would be of much interest to examine, in future investigations, whether the five M-Chl *a*s are photoactive or not in other photochemical systems (*e.g.*, a photocatalytic system using a molecular donor or acceptor).

A Kinetic Study with Mixed M-Chl *a* Monolayers

The five non-sensitizing M-Chl *a*s behave quite normal with respect to monolayer formation as well as optical absorption characteristics. We can thus prepare a mixed monolayer composed of a sensitizing M_1-Chl *a* and a non-sensitizing M_2-Chl *a* on the SnO_2 substrate. If an energy transfer takes place from excited M_1-Chl *a* to ground-state M_2-Chl *a*, the net photocurrent quantum yield Φ_s will decrease due to a rapid energy degradation within the M_2-Chl *a* molecule. A close examination of such a quenching behavior will provide useful information regarding the kinetic features of the interfacial photoprocess.

A typical example demonstrating the occurrence of photocurrent quenching is depicted in Fig. 10. The open circle represents the sensitized photocurrent at a SnO_2 electrode coated with Pd-Chl *a* alone, and the filled circle represents that at a SnO_2 electrode coated with a mixture of Pd-Chl *a* and Ni-Chl *a*. The heights of the 640-nm photocurrent maxima give relative quantum yields. It is readily seen that the coexistence of Ni-Chl *a* has significantly quenched the Pd-Chl *a* - sensitized photocurrent.

In what follows the results of such quenching experiments, in which Cu-, Pd-, and Mg-Chl *a* are used as M_1-Chl *a* (sensitizer) and Ni-Chl *a* as M_2-Chl *a* (quencher),

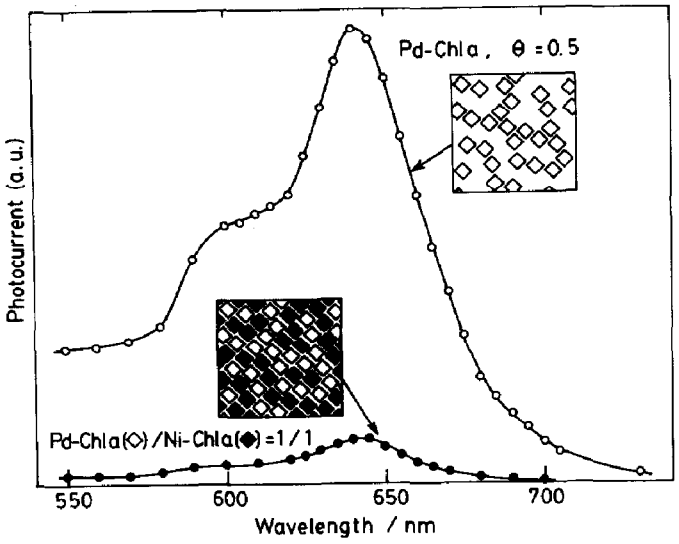

Fig. 10 Sensitized photocurrent spectra at SnO_2 electrodes coated with a Pd-Chl *a* monolayer ($[\text{Pd-Chl } a]_s = 5.0 \times 10^{13}$ molecules cm^{-2}, adjusted with DPL) (○), and with a Pd-Chl *a* / Ni-Chl *a* mixed monolayer ($[\text{Pd-Chl } a]_s = [\text{Ni-Chl } a]_s = 4.72 \times 10^{13}$ molecules cm^{-2}) (●).

are presented briefly. To study the dependence of the quenching effect on the sensitizer - quencher separation, the surface concentration was varied by use of DPL as a diluent. In each measurement, the ratio of surface population $[M_1\text{-Chl } a]_s/[M_2\text{-Chl } a]_s$ was adjusted to 1.0.

Cu-Chl *a*. The Cu-Chl *a* - sensitized photocurrent is suppressed by the presence of Ni-Chl a in the monolayer, as shown in Fig. 11. Since Cu-Chl *a* appears to inject an electron into SnO_2 from the triplet excited state (see above), we suppose that the latter state is quenched by Ni-Chl *a* via triplet-triplet energy transfer. Denoting Cu-Chl *a* and Ni-Chl *a* by P and Q, respectively, the following schemes are assumed for the interfacial photoprocess:

$$P + h\nu \longrightarrow {}^1P^* \longrightarrow {}^3P^* \quad \text{(excitation and intersystem crossing)} \tag{1}$$

$${}^3P^* \xrightarrow{k_s} P^+ + e^- \quad \text{(electron transfer into } SnO_2\text{)} \tag{2}$$

$${}^3P^* \xrightarrow{k_d} P \quad \text{(deactivation)} \tag{3}$$

$${}^3P^* + Q \longrightarrow P + {}^3Q^* \longrightarrow P + Q \quad \text{(energy transfer quenching)} \tag{4}$$

The rate constant for process (4) is assumed to have a simple form (ref. 22) $k_Q \exp(-bd)$, where d (cm) is the average intermolecular distance and b is a constant. The value of d is related to C, the Cu-Chl *a* surface concentration (in

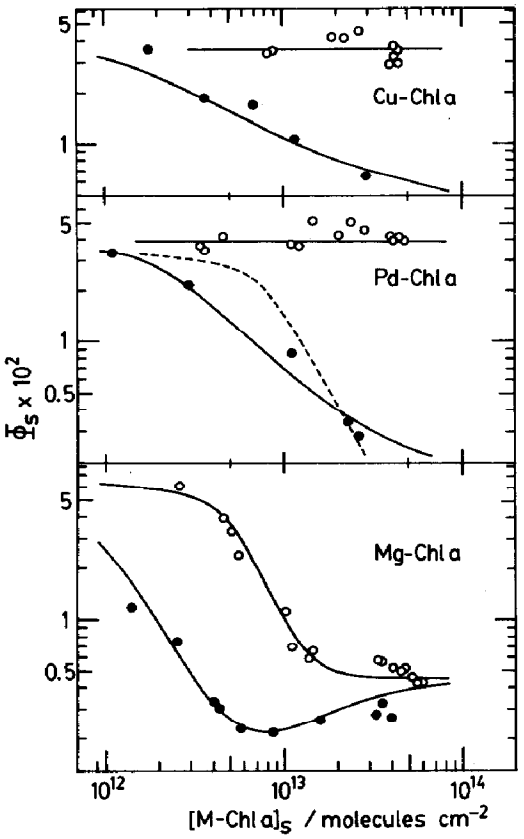

Fig. 11 Photocurrent quantum yield (Φ_s) vs. surface concentration ([M-Chl *a*]$_s$) profiles for Cu-, Pd-, and Mg-Chl *a* monolayers in the absence (o) and presence (●) of added Ni-Chl *a* to a 1:1 molar ratio. The abscissa denotes the surface concentration of a sensitizing M-Chl *a* alone. For Pd-Chl *a*, the solid curve through the filled circles is drawn by assuming triplet-triplet quenching, and the dashed curve represents singlet-singlet quenching.

molecules cm^{-2}), by the equation:

$$2\pi d^2 C = 1 \qquad (5)$$

The factor 2 comes from the fact that the total pigment concentration is twice the sensitizer concentration. Under these assumptions the photocurrent quantum yield Φ_s is given by

$$\Phi_s = k_s / [k_s + k_d + k_Q \exp(-b / \sqrt{2\pi C})] \qquad (6)$$

or

$$\Phi_s^{-1} = \frac{k_s + k_d}{k_s} + \frac{k_Q}{k_s} \exp(-b / \sqrt{2\pi C}) \qquad (7)$$

The value of Φs in the absence of Ni-Chl *a* is 0.035, hence $(k_s + k_d)/k_s = 28.6$, or

$k_d/k_s = 27.6$. A computer simulation of the quenching data in Fig. 11 by means of eq. (7) gives a best-fit curve with the following values: $k_Q/k_s = 0.308$ and $b = 1.04 \times 10^7$ cm^{-1}.

Pd-Chl *a*. Since Pd-Chl *a* is, though only weakly, fluorescent, both the triplet-triplet and singlet-singlet mechanisms can be envisaged for the photocurrent quenching by Ni-Chl *a*. At present we are unable to distinguish between these two possibilities. In case where the triplet mechanism is assumed, we can treat the quenching data again in terms of eq. (7) and obtain a simulated curve (solid curve through filled circles in Fig. 11) with parameters $k_Q/k_s = 1.20$ and $b = 1.71 \times 10^7$ cm^{-1}.

In the case of singlet-singlet (Förster) quenching, processes (1) - (4) are replaced by

$$P + h\nu \longrightarrow {}^1P^* \qquad \text{(excitation)} \tag{8}$$

$${}^1P^* \xrightarrow{k_s} P^{+}\cdot + e^- \qquad \text{(electron injection)} \tag{9}$$

$${}^1P^* \xrightarrow{k_d} P \qquad \text{(deactivation)} \tag{10}$$

$${}^1P^* + Q \xrightarrow{k_{en}} P + {}^1Q^* \longrightarrow P + Q \qquad \text{(quenching)} \tag{11}$$

A difficulty arises in evaluating the rate constant k_{en} for process (11). The decay profile $D(t)$ of an excited singlet state in the presence of two-dimensional Förster-type energy transfer (ref. 23) is given by

$$D(t) = \exp\left[-\frac{t}{\tau_f} - \Gamma\left(\frac{2}{3}\right)\frac{n}{n_0}\left(\frac{t}{\tau_f}\right)^{1/3}\right] \tag{12}$$

where $\Gamma(\frac{2}{3}) = 1.354$, τ_f $(= 1/k_f)$ is the fluorescence lifetime in the absence of energy transfer, n the surface concentration (molecules cm^{-2}) of the acceptor, and n_0 the critical surface concentration of the acceptor defined by

$$\pi R_0^{\,2} n_0 = 1 \tag{13}$$

Here R_0 is the critical distance (cm) for ${}^1P^* \rightarrow Q$ energy transfer. Thus, k_{en} in process (11) cannot be uniquely determined. To overcome this difficulty, we use a formalism for fluorescence quantum yield. If we denote the fluorescence quantum yield in the presence and absence of energy transfer quenching by Φ_f and $\Phi_f{}^0$, respectively, the following equation should hold:

$$\Phi_f/\Phi_f{}^0 = \int_0^\infty D(t)dt \Big/ \int_0^\infty \exp(-t/\tau_f)\,dt \tag{14}$$

$$= 1 - \sigma\int_0^\infty \exp(-u^3 - \sigma u)du \tag{15}$$

with

$$\sigma = \Gamma\left(\frac{2}{3}\right)\frac{n}{n_0} \tag{16}$$

We then approximate eq. (15) formally by

$$\Phi_f/\Phi_f^o = k_f / (k_f + k_{en}) \qquad (18)$$

to define a time-averaged energy transfer rate constant, k_{en} (s^{-1}).

From the fluorescence spectrum of Pd-Chl *a* and absorption spectrum of Ni-Chl *a* (measured in acetone) we evaluate R_o to be 2.2×10^{-7} cm, corresponding to n_o = 6.6×10^{12} molecules cm^{-2}. At an arbitrary Ni-Chl *a* surface concentration n, σ is obtained from eq. (16). Then eq. (15) is numerically solved to obtain a value of Φ_f/Φ_f^o, which in turn gives a formal value of k_{en} by eq. (18) using $k_f = 2 \times 10^{10}$ s^{-1} (see above). The dashed curve in Fig. 11 represents the photocurrent quantum yield

$$\Phi_s = k_s / (k_s + k_d + k_{en}) \qquad (19)$$

with k_{en} evaluated as described above as a function of $[\text{Ni-Chl } a]_s$ (= $[\text{Pd-Chl } a]_s$). As a result of this procedure, the value of k_s (rate constant for electron injection from the singlet excited state of Pd-Chl *a* into the CB of SnO_2) was obtained to be 1.6×10^9 s^{-1}.

In the analysis described above, the values used as R_o and k_f are those estimated from the optical data acquired in organic solutions. For a more reliable treatment these should be measured directly at the adsorbed state.

Mg-Chl *a*. The photocurrent quantum yield Φ_s for the Mg-Chl *a* monolayer containing Ni-Chl *a* exhibits a rather complicated dependence on the surface concentration, in constrast to a monotonic change observed in cases of Cu-Chl *a* and Pd-Chl *a* (Fig. 11). At concentrations near the compact monolayer (right-hand end of Fig. 11), the Φ_s for the mixed monolayer is at a level close to that of Φ_s in the absence of Ni-Chl *a*. Qualitatively this is understood by assuming that an energy transfer from Mg-Chl *a* dimers, supposed to exist predominantly at higher surface concentrations, to the quencher (Ni-Chl *a*) is very inefficient. Dimers absorb at longer wavelengths and are much less fluorescent than the monomer; this would result in a decreased probability of the Förster-type energy transfer to Ni-Chl *a*. With decreasing $[\text{Mg-Chl } a]_s$, the Φ_s value in the presence of Ni-Chl *a* tends to decrease to reach a minimum value of 0.002 at $[\text{Mg-Chl } a]_s \simeq 7 \times 10^{12}$ molecules cm^{-2}. Such a decrease comes most probably from an increasing fraction of the monomeric Mg-Chl *a*, whose singlet excited state can be quenched efficiently via a Förster energy transfer to Ni-Chl *a*. On further dilution of the monolayer, the Φ_s value shows an increase toward the non-quenched level, due to an increase in the Mg-Chl *a* - Ni-Chl *a* intermolecular separation.

A quantitative analysis of the quenching data for the Mg-Chl *a* + Ni-Chl *a* mixed monolayer / SnO_2 system is currently in progress, and the result will be reported elsewhere (ref. 24).

CONCLUDING REMARKS

Our results show that Mg-Chl *a*, among a series of M-Chl as, has the highest ability of electron releasing from the singlet excited state *if quenching processes are effectively suppressed*. This property appears essential for the initial event at the reaction center, which has to transfer an electron over a distance of about 50 Å (from the inner to outer side of the thylakoid membrane) at the expense of an energy loss of as much as 0.8 eV (ref. 25).

ACKNOWLEDGMENTS

The authors are grateful to Drs. K. Itoh and A. Fujishima for stimulating discussions, and to Mr. M. Yamamoto for his participation in the experiments. They also thank Mrs. M. Nakazato, M. Konno, and S. Saitoh, Nampo Pharmaceutical Co., Ltd., for continuous supply of Mg-Chl *a*.

REFERENCES

1 B.D.Berezin and N.I.Sosnikova, Russ. J. Phys. Chem., 38 (1964) 663-666.
2 B.D.Berezin and A.N.Drobysheva, Russ. J. Phys. Chem., 44 (1970) 1597-1601.
3 B.L.Baker and G.W.Hodgson, J. Phys. Chem., 65 (1961) 1078-1079.
4 I.D.Jones, R.C.White, E.Gibbs and C.D.Denard, J. Agr. Food Chem., 16 (1968) 80-83.
5 J.J.Katz and J.C.Hindman, in J.S.Connolly (ed.), Photochemical Conversion and Storage of Solar Energy, Academic Press, New York, 1981, pp.27-78.
6 W.A.Svec in D.Dolphin (ed.), The Porphyrins, Vol. 5, Academic Press, New York, 1978, pp.341-399.
7 T.Watanabe, H.Suzuki, K.Machida, M.Kobayashi, N.Obi, M.Yamamoto and K.Honda, to be published.
8 K.Itoh, R.Baba, T.Watanabe, H.Suzuki and K.Honda, to be published.
9 T.Watanabe, H.Suzuki, M.Kobayashi, N.Obi and K.Honda, to be published.
10 T.Watanabe, A.Hongu, Y.Aoyagi and K.Honda, to be published.
11 T.Watanabe, T.Miyasaka, A.Fujishima and K.Honda, Chem. Lett., (1978) 443-446.
12 T.Miyasaka, T.Watanabe, A.Fujishima and K.Honda, J. Am. Chem. Soc., 100 (1978) 6657-6665.
13 F.J.Kampas, K.Yamashita and J.Fajer, Nature (London), 284 (1980) 40-42.
14 K.Uehara, Y.Nakajima, M.Yonezawa and M.Tanaka, Chem. Lett., (1981) 1643-1646.
15 T.Watanabe, A.Fujishima and K.Honda, in M.Grätzel (ed.), Energy Resources through Photochemistry and Catalysis, Academic Press, New York, 1983, pp.359-384.
16 M.Nakao, K.Itoh, T.Watanabe and K.Honda, Ber. Bunsenges. Phys. Chem., in press.
17 J.-H.Fuhrhop, in K.M.Smith (ed.), Porphyrins and Metalloporphyrins, Elsevier, Amsterdam, 1975, pp.593-623.
18 R.H.Felton, in D.Dolphin (ed.), The Porphyrins, Vol. 5, Academic Press, New York, 1978, pp.53-125.
19 T.Watanabe, M.Kimura and K.Honda, Denki Kagaku, 50 (1982) 394-400.
20 T.Watanabe and K.Honda, J. Phys. Chem., 86 (1982) 2617-2619.
21 T.Kobayashi, K.D.Straub and P.M.Rentzepis, Photochem. Photobiol., 29 (1979) 925-931.
22 D.L.Dexter, J. Chem. Phys., 21 (1953) 836-850.
23 N.Nakashima, K.Yoshihara and F.Willig, J. Chem. Phys., 73 (1980) 3553-3559.
24 T.Watanabe, K.Machida and K.Honda, to be published.
25 H.T.Witt, Biochim. Biophys. Acta, 505 (1979) 355-427.